





RESEARCH PAPER

 OPEN ACCESS 

## Staufen1 unwinds the secondary structure and facilitates the translation of fatty acid binding protein 4 mRNA during adipogenesis

Xiaodi Liang <sup>a,\*</sup>, Yi Jiao<sup>a,\*</sup>, Xueli Gong<sup>b</sup>, Hao Gu<sup>c</sup>, Nuerbiye Nuermaiti<sup>a</sup>, Xuanyu Meng<sup>a</sup>, Dihui Liu<sup>a</sup>, and Yaqun Guan <sup>a</sup>

<sup>a</sup>State Key Laboratory of Pathogenesis, Prevention and Treatment of High Incidence Diseases in Central Asia, Department of Biochemistry and Molecular Biology, Preclinical Medicine College, Xinjiang Medical University, Urumqi, Xinjiang, China; <sup>b</sup>Department of Pathophysiology, Preclinical Medicine College, Xinjiang Medical University, Urumqi, Xinjiang, China; <sup>c</sup>Department of Laparoscopic Surgery, First Affiliated Hospital, Xinjiang Medical University, Urumqi, Xinjiang, China

### ABSTRACT

Adipogenesis is regulated by genetic interactions, in which post-transcriptional regulation plays an important role. Staufen double-stranded RNA binding protein 1 (Staufen1 or *STAU1*) plays diverse roles in RNA processing and adipogenesis. Previously, we found that the downregulation of *STAU1* affects the expression of fatty acid-binding protein 4 (*FABP4*) at the protein level but not at the mRNA level. This study aimed to determine the mechanism underlying the regulation of *FABP4* expression by *STAU1*, explaining the inconsistency between *FABP4* mRNA and protein levels. We used RNA interference, photoactivatable ribonucleoside enhanced cross-linking and immunoprecipitation, and an adeno-associated virus to examine the functions of *STAU1* in adipogenesis. Our results indicate that *STAU1* binds to the coding sequences of *FABP4*, thereby regulating the translation of *FABP4* mRNA by unwinding the double-stranded structure. Furthermore, *STAU1* mediates adipogenesis by regulating the secretion of free fatty acids. However, *STAU1* knockdown decreases the fat weight/body weight ratio but does not affect the plasma triglyceride levels. These findings describe the mechanisms involved in *STAU1*-mediated regulation of *FABP4* expression at the translational level during adipogenesis.

### ARTICLE HISTORY

Received 7 June 2021  
Accepted 21 June 2021

### KEYWORDS

Staufen1; adipogenesis; fatty acid binding protein 4; lipid metabolism; RNA processing



## Introduction

The adipose tissue is a metabolic organ that plays critical roles in the regulation of energy homeostasis and lipid metabolism [1,2]. Adipocyte differentiation involves different levels of gene expression [3,4]. During translation, the secondary structure of mRNA affects translation efficiency, and higher levels of RNA binding proteins regulate this process [5,6].

Staufen double-stranded RNA binding protein 1 (Staufen1/*STAU1*) is a double-stranded RNA (dsRNA)-binding protein that can recognize the Staufen binding sites (SBS) and affect the structure, translation efficiency, and degradation of mRNA [7–9]. Nearly all double-stranded RNAs are recognized and bound by *STAU1* [10], the expression of which is upregulated during adipogenesis [11]. In our previous study, we demonstrated that nearly 3,000 different mRNA species are upregulated upon downregulation of *STAU1* expression during adipogenesis. Recent studies have

indicated that *STAU1* can sense the secondary structure of mRNA and regulate translation [10].

Previously, we have shown that mRNAs of fatty acid-binding protein 4 (*FABP4*) possess SBS in their open reading frames; this finding indicates that *STAU1* may regulate the expression of *FABP4* [12]. *FABP4*, also called adipocyte protein 2, is a lipid chaperone [13]. *FABP4* encodes the 14 kD protein FABP4, which binds to fatty acids and facilitates the transportation of fatty acids to different organelles [14,15]. During adipogenesis, *FABP4* is transcribed by different transcription factors such as peroxisome proliferator-activated receptor  $\gamma$  (*PPAR\gamma*) and CCAAT/enhancer-binding protein  $\alpha$  (*C/EBP\alpha*) [16]. *PPAR\gamma* can recognize a specific motif in the promoter of *FABP4* and enhance *FABP4* transcription. However, high levels of *FABP4* can trigger the degradation of *PPAR\gamma*, thereby downregulating *PPAR\gamma* levels [17]; this indicates a post-transcriptional regulation mechanism that regulates the expression of *FABP4*.

**CONTACT** Yaqun Guan  [yaqunguan557@xjmu.edu.cn](mailto:yaqunguan557@xjmu.edu.cn)  State Key Laboratory of Pathogenesis, Prevention and Treatment of High Incidence Diseases in Central Asia, Department of Biochemistry and Molecular Biology, Preclinical Medicine College, Xinjiang Medical University, Urumqi, Xinjiang, China  
\*Xiaodi Liang and Yi Jiao contributed equally to this work.

© 2021 The Author(s). Published by Informa UK Limited, trading as Taylor & Francis Group.  
This is an Open Access article distributed under the terms of the Creative Commons Attribution License (<http://creativecommons.org/licenses/by/4.0/>), which permits unrestricted use, distribution, and reproduction in any medium, provided the original work is properly cited.

In this study, we used siRNAs to downregulate the expression of *STAU1* to evaluate its function in adipogenesis. Furthermore, we sought to elucidate the mechanisms underlying *STAU1*-mediated expression of *FABP4*.

## Results

### *Inhibition of STAU1 downregulates the expression of FABP4*

3T3-L1 cells were induced with an adipogenic cocktail and then used to examine the differentiation of preadipocytes into adipocytes. siRNA1 and siRNA2 were used to downregulate *STAU1* as described previously [18]. Our results indicate that expression of *STAU1* is significantly downregulated by  $1.7 \pm 0.57$ -fold for siRNA1 and by  $2.1 \pm 0.48$ -fold for siRNA2 ( $P < 0.05$ ,  $n = 3$ ) compared with that of the negative control (NC) (Figure 1(a,e,f)). We next analysed the mRNA and protein levels of *C/EBP $\alpha$* , *PPAR $\gamma$* , and *FABP4*. Our results revealed that *C/EBP $\alpha$*  and *PPAR $\gamma$*  mRNA (Figure 1(b,c)) and protein levels (Figure 1(e,g,h)) are downregulated after the knockdown of *STAU1*. Moreover, the levels of *FABP4* decrease, while its mRNA levels remain unchanged (Figure 1(d,e,i)). These results suggest that *STAU1* may regulate the expression of *FABP4* at the post-transcriptional level.

### *STAU1 binds to the SBS of FABP4 mRNA*

We next used RIP to evaluate the binding of *STAU1* to *FABP4* mRNA. After precipitating *FABP4* mRNA with a *STAU1* antibody and IgG, we found that *STAU1* could successfully pull down the *FABP4* mRNA, but not IgG (Figure 2(a)). A previous study has shown that *STAU1* recognizes and binds to different SBS at different positions [10]. A typical SBS contains a stem-loop structure; therefore, we used an online database to predict the secondary structure of *FABP4* mRNA [19]. The nucleotide sequence of mouse *FABP4* mRNA, obtained from NCBI (NM\_024406.3), contains 696 bases and a coding region of 106–504 base pairs. Analysis of the secondary structure of *FABP4* mRNA revealed at least four putative SBS, as shown in Figure 2(c). Among these four positions, 2–4 were located in the coding sequences (CDS) of *FABP4* mRNA; while, position 1 was located in the 5' UTR. To further investigate which position is recognized by *STAU1*, we used photoactivatable ribonucleoside enhanced cross-linking and immunoprecipitation (PAR-CLIP) to proliferate different positions of *FABP4* mRNA via different primers (Figure 2(b)). Our results, obtained using qRT-

PCR, show that *STAU1* is able to recognize and bind position 3 (110–220) (Figure 2(d)). These findings suggested that *STAU1* positively regulated the levels of *FABP4* predominantly at the post-transcriptional level by directly binding to *FABP4* mRNA in the coding region.

### *STAU1 facilitates the translation of FABP4*

*STAU1* can bind to the CDS of mRNA and facilitate translation [10]. Considering that *STAU1* is capable of binding to *FABP4* mRNA, we hypothesized that *STAU1* may promote the ribosome occupancy of *FABP4*. To further elucidate the effects of *STAU1* on *FABP4* RNA, we used a sucrose gradient to fractionate cytoplasmic mRNAs. Two siRNAs were used to downregulate *STAU1* to avoid off-target effects in differentiated 3T3-L1 cells on day 4. Our results indicate that after the downregulation of *STAU1*, ribosome distribution changes significantly; polysome distribution is notably affected, while the percentage of monoribosomes increases significantly (Figure 3(a)). These results indicate that *STAU1* may regulate ribosome and polysome stalling. We then compared the expression profile of *FABP4* mRNAs along each gradient. Expectedly, qRT-PCR revealed enrichment in endogenous *FABP4* transcript levels in polysomal fractions from *STAU1*-knockdown cells compared with the levels of the controls. We also observed that *FABP4* mRNAs shifts towards the monoribosome fraction after *STAU1* knockdown via both siRNAs (Figure 3(b)). *STAU1* facilitates translation by unwinding the secondary structure of mRNA via p-UPF1, which is an ATPase-dependent helicase. Therefore, we used OA to retain UPF1 in a hyperphosphorylated state [20]. After 3T3-L1 cells were treated with OA, the expression of *FABP4* protein increases significantly whereas *FABP4* mRNA levels do not change compared with the levels in the DMSO-treated controls (Figure 3(c-e)). These results indicate that *STAU1* protein regulate the expression of *FABP4* at the translational level.

### *STAU1 attenuates adipogenesis by mediating the expression of FABP4*

*FABP4* is a marker of adipogenesis. We sought to evaluate the function of *STAU1* in lipid drop formation. Thus, we examined adipogenesis in *STAU1*-downregulated cells. Oil Red O was used to stain 3T3-L1 cells in which *STAU1* was downregulated via siRNAs, and which were induced to differentiate into adipocytes on different days. Our results showed that lipid droplets in 3T3-L1 cells are significantly decreased

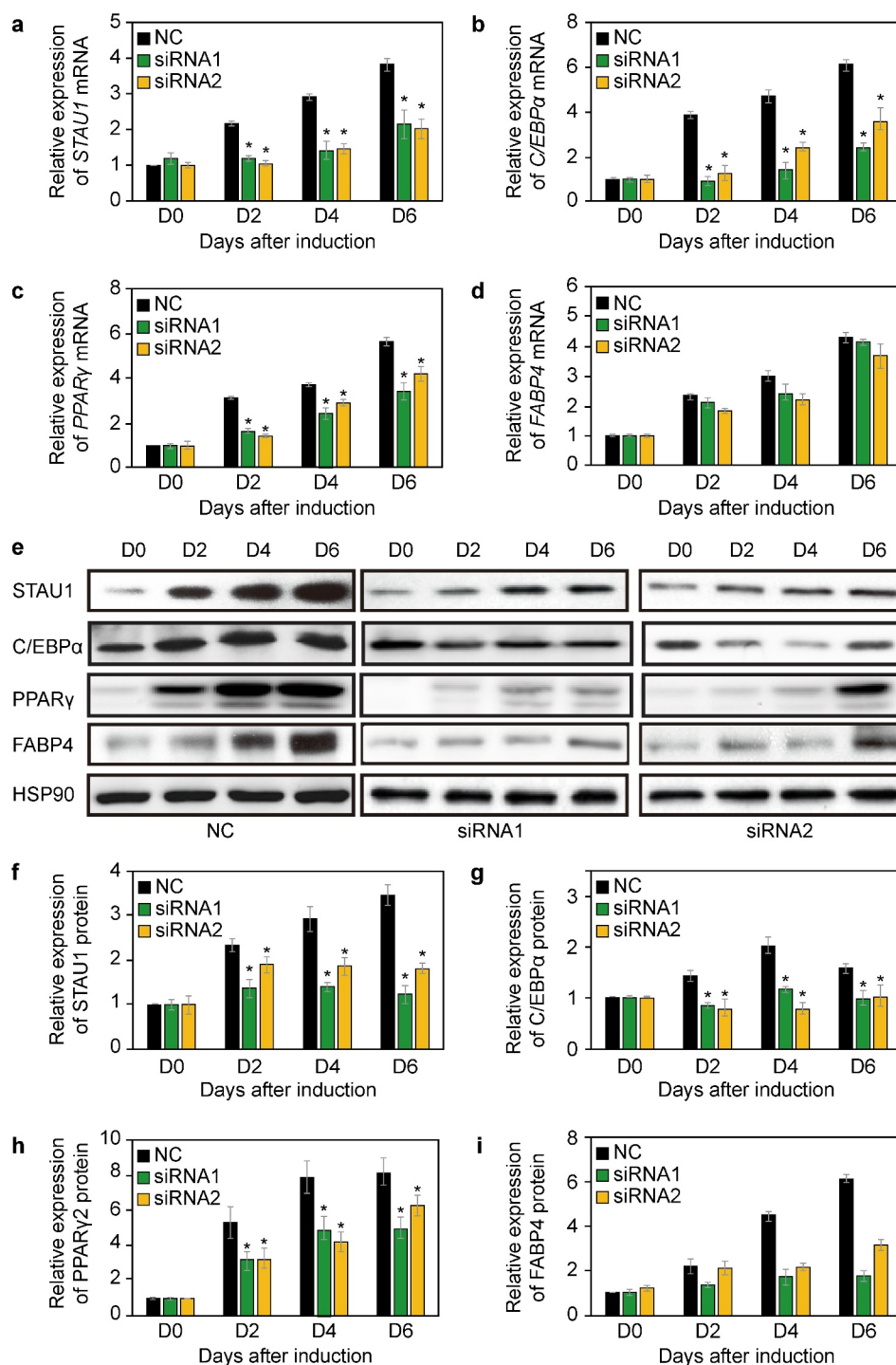


**Figure 1.** Expression of *STAU1*, *C/EBPα*, *PPARγ*, and *FABP4* after downregulation of *STAU1*. A-D: qPCR quantification of *STAU1*, *C/EBPα*, *PPARγ*, and *FABP4* mRNA levels on days 2, 4, and 6, as compared to the levels at day 0. E: Western blot was used to assess the levels of *STAU1*, *C/EBPα*, *PPARγ*, and *FABP4* on days 2, 4, and 6; these levels were compared with those of negative control (NC). F-I: Quantification of *STAU1*, *C/EBPα*, *PPARγ*, and *FABP4* expression levels assessed via western blotting on days 2, 4, and 6 and compared to the levels at day 0. The results are presented as the mean  $\pm$  standard deviation (\* $P < 0.05$ , compared with NC).

after downregulation of *STAU1* (Figure 4(a)). The absorption of 3T3-L1 cell lysates, obtained after oil red O staining, was then measured at 495 nm using a spectrophotometer. Our results revealed that adipogenesis is significantly decreased after downregulation

of *STAU1* (Figure 4(b)). Because *FABP4* facilitates fatty acid transportation, we next assessed the secretion of *FABP4* to evaluate fatty acid metabolism. 3T3-L1 cells were induced using the induction cocktail for 4 days and then transfected with *STAU1* siRNAs. We found

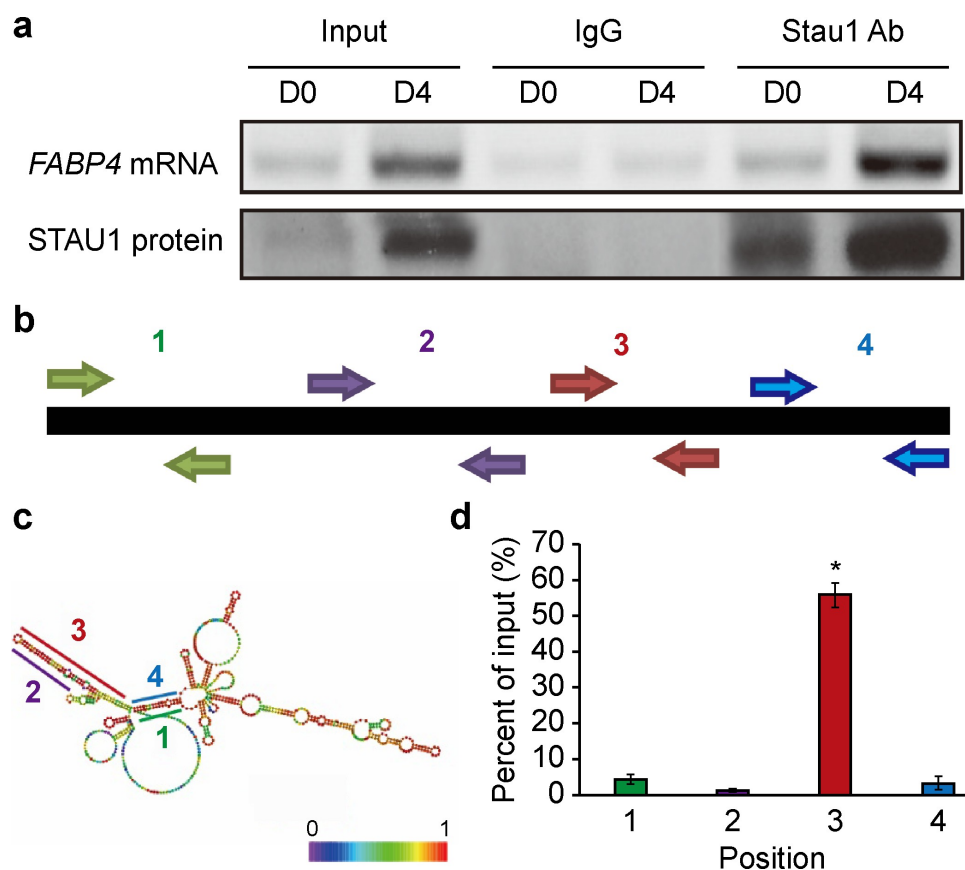


**Figure 2.** Binding of STAU1 to the CDS of *FABP4*. **A:** Results obtained using RT-PCR show the expression of *FABP4* mRNA precipitated by IgG or STAU1 antibody at 0- and 4-days post-induction. Western blot showing specific IPs of STAU1 at 0- and 4-days post-induction. **B:** The schematic shows PAR-CLIP primers designed for the different positions. **C:** Secondary structure of *FABP4* mRNA. Different putative SBS are indicated by different numbers. **D:** Results obtained via qPCR show the percentage of STAU1 binding to *FABP4* mRNA at different positions as compared with input *FABP4* mRNA. The results are presented as the mean  $\pm$  standard deviation.

that *FABP4* was present in both the cell lysates (CL) and cell medium (CM), while *GAPDH*, which is not a secretory protein, was not present in the CM. The levels of *FABP4* levels in the CM and CL were significantly decreased after downregulation of STAU1, indicating that STAU1 may regulate fatty acid transport during adipogenesis. In addition, the glycerol and free fatty acid (FFA) content is markedly decreased in the CM after downregulation of STAU1 (Figure 4(d-e)). These results indicate that STAU1 regulates the lipid drop formation and lipid metabolism *in vitro*.

### Overexpression of STAU1 in subcutaneous fat of mice increases weight and lipid metabolism

To examine the function of STAU1 *in vivo*, we generated an adeno-associated virus (AAV) encoding scrambled siRNA (AAV-Control) and siRNA designed according to the sequence of siRNA1 (AAV-*shSTAU1*), which targets *STAU1* mRNA. qRT-PCR show that AAV-*shSTAU1* knocks down the expression of *STAU1*

mRNA (Figure 5(a)) in the adipose tissue of the HFD-fed mice by 62% compared with the expression levels of the wild-type (WT) mice fed a standard chow (SC) ( $5 \pm 2$  animals per group). Wild-type diet-induced obese mice that had been fed an HFD showed a 65% decrease in *STAU1* expression in the adipose tissue compared with that of WT mice. Considering that STAU1 regulates the expression of *FABP4* *in vitro*, we performed qRT-PCR to measure *FABP4* levels in SC- and HFD-fed mice treated with AAV-control and AAV-*shSTAU1*. The expression of *FABP4* mRNA did not change in SC- and HFD-fed mice after downregulation of *STAU1* (Figure 5(b)). We then used western blotting to examine the expression of *STAU1* and *FABP4* in the adipose tissue of mice treated with AAV-control or AAV-*shSTAU1* compared with that of the control mice. In agreement with the *in vitro* results, the levels of *STAU1* and *FABP4* proteins were decreased in SC- and HFD-fed mice after expression of *STAU1* was knocked down by AAV-*shSTAU1*. Furthermore, the mRNA and protein levels of *STAU1* and *FABP4* were

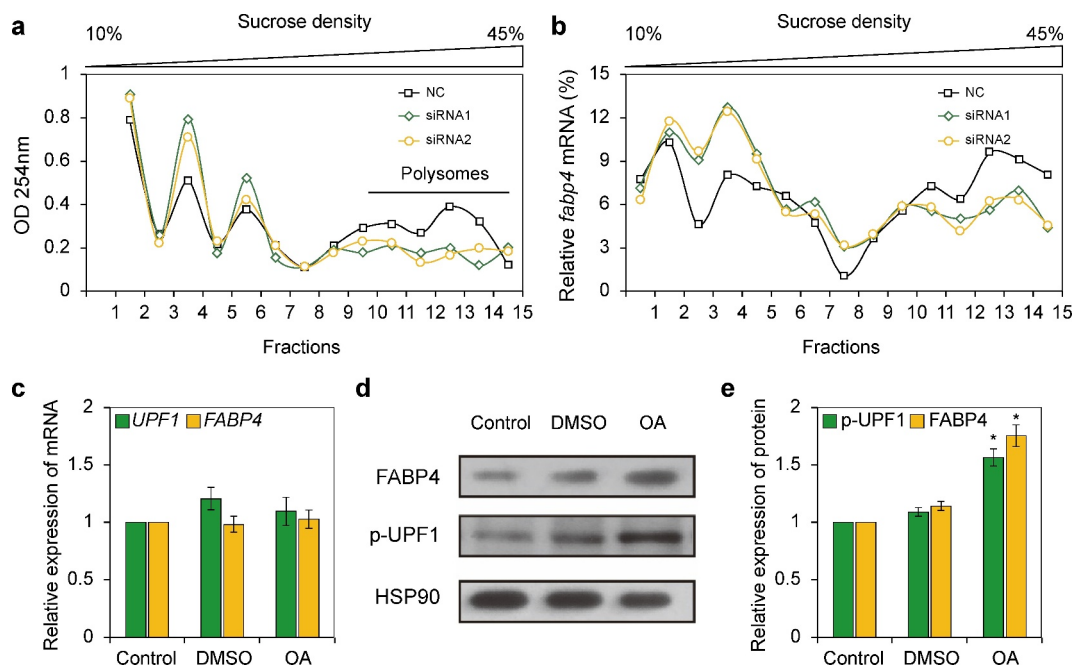


**Figure 3.** STAU1 upregulates the expression of FABP4 protein. A. Polysome profiling of 3T3-L1 cells on day 4 post-induction, obtained by the continuous reading of absorbance at 254 nm after downregulation of STAU1. B. Levels of *FABP4* mRNA were measured by qRT-PCR using 15 sucrose gradient fractions obtained after downregulation of STAU1 and on day 4 post-induction. C. 3T3-L1 cells were treated with 0.1  $\mu$ M okadaic acid on day 4 post-induction; then, the *UPF1* and *FABP4* mRNA expressions were quantified by RT-qPCR. DMSO-treated 3T3-L1 cells were used as controls. D-E: Western blot showing the expression of STAU1 and FABP4 protein in OA-treated, DMSO-treated, and untreated 3T3-L1 cells.

increased in HFD-fed mice compared with those in SC-fed mice. To characterize the functional impact of STAU1 knockdown, we analysed the bodyweight of SC- and HFD-fed mice. At week 10, the body weights of AAV-*shSTAU1* SC-fed mice were reduced compared with the body weights of SC-fed WT mice; this difference in the body weights of the mice groups was maintained throughout the remainder of our 8-week study. Half of the mice were switched to HFD at 9 weeks of age. After 6 weeks of consuming HFD, AAV-*shSTAU1* mice showed a significant increase in body weight compared with that of HFD-fed WT mice; however, downregulation of STAU1 decreased the body weights of AAV-*shSTAU1* mice fed HFD.

We then used quantitative nuclear magnetic resonance to examine whole-body fat mass in the different mouse cohorts. In both SC- and HFD-fed mouse cohorts, body fat content is significantly decreased in mice treated with AAV-*shSTAU1* compared with that of WT (Figure 5(g)). However, WT mice fed HFD demonstrate an almost four-fold increase in fat mass compared with that of SC-fed mice. Taken together, our data indicate that knockdown of *STAU1* robustly decreases the body weight and fat mass of HFD-fed mice. To investigate the potential physiological effects of *STAU1* knockdown, we analysed key plasma

metabolic parameters in mice fed *ad libitum* or fasted overnight. As shown in Figure 5(h), triglyceride (TG) levels do not differ in SC-fed mice treated with AAV-*shSTAU1* or AAV-control. Furthermore, TG levels also remain unchanged in the different groups of HFD-fed mice. However, plasma TG levels of HFD-fed mice are increased compared with those of SC-fed mice. These results indicate that STAU1 regulates body weight and fat tissue accumulation in mice without affecting the levels of plasma TG.

## Discussion

Similar to other RNA-binding proteins, STAU1 participates in RNA surveillance, localization, and translation, as well as in alternative splicing during post-transcriptional processing [7,21,22]. During the translation of mRNA, secondary structures such as hairpins, stems, and loop can interfere with translation mechanisms [23]. In this study, we analysed the secondary structure of *FABP4* and found that STAU1 bound to the SBS of *FABP4* and facilitated *FABP4* translation. Knockdown of STAU1 affected the expression of *FABP4* both *in vitro* and *in vivo*. We next examined the function of STAU1 in adipocytes and adipose tissue

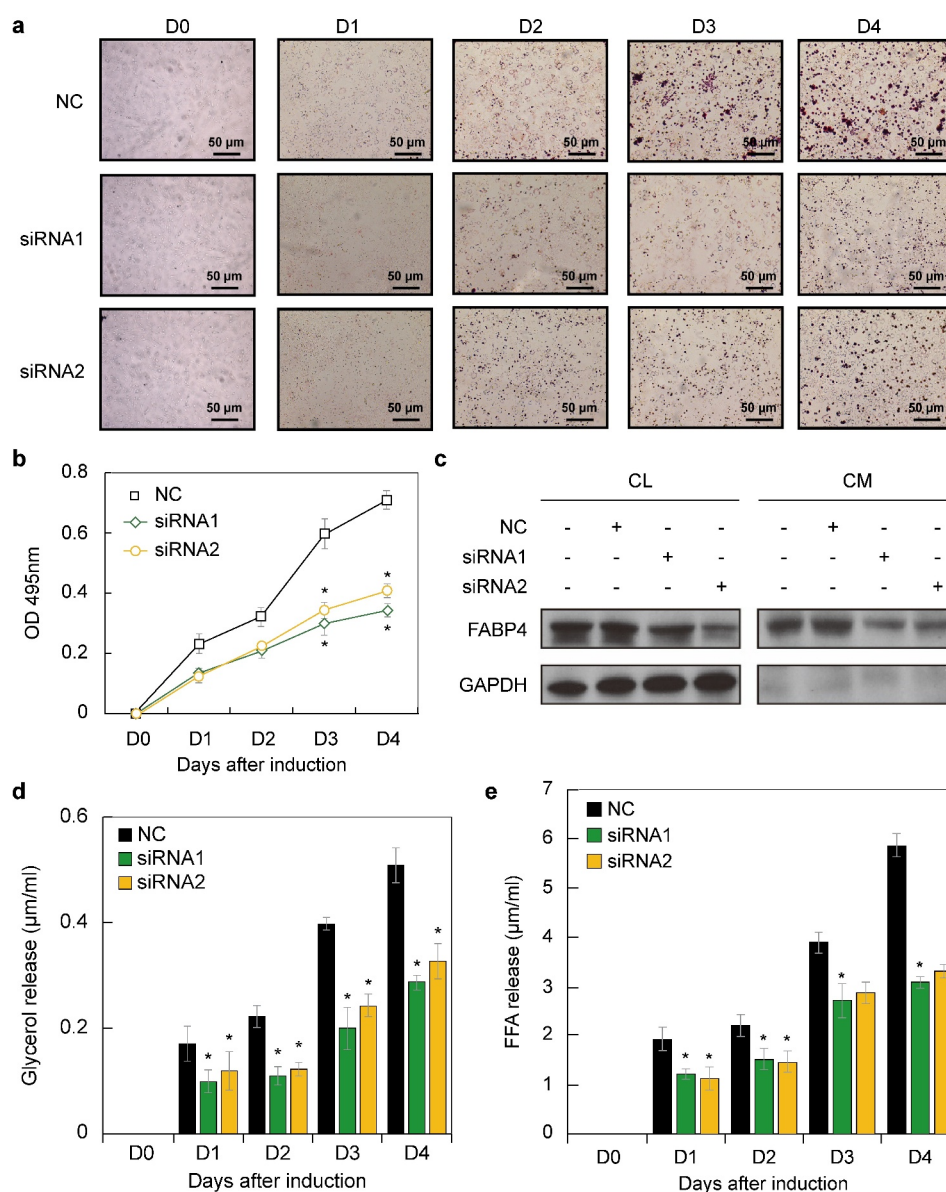


**Figure 4.** STAU1 regulates adipogenesis. A. Representative images of oil red O-stained 3T3-L1 cells at days 0, 1, 2, and 3. Scale bar, 50  $\mu\text{m}$ . B. Lipid accumulation was assessed at 495 nm in 3T3-L1 cells stained with oil red O and de-stained with isopropyl alcohol ( $n = 3$ ). C. Glycerol content in the cell culture medium ( $n = 3$ ). F. FFA content in the cell culture medium ( $n = 3$ ). FFA: free fatty acid. Values are expressed as means  $\pm$  SEM vs. control group, \*  $P < 0.05$ .

and found that STAU1 regulated adipogenesis and adipose development by regulating the expression of FABP4.

The expression of FABP4 is highly induced during adipogenesis and is transcriptionally controlled by PPAR $\gamma$  and C/EBP $\alpha$  [17]. The transcribed FABP4 mRNA is spliced and transported to the cytoplasm to be translated into protein [24]. During these processes, secondary structures of mRNAs can greatly influence translation efficiency [25]. Certain structures within mRNAs can be recognized by RNA-binding proteins and they can affect the initiation and termination of translation or RNA decay [26]. In this study, we found

four potential SBS in FABP4 mRNA. Using PAR-CLIP, we verified that the SBS in position 3 could be recognized and bound by STAU1. This SBS in position 3 is located 110–220 nt from FABP4 mRNA, which is located in the CDS region. It is possible that STAU1 binds to this region and recruits other RNA-binding proteins, such as regulator of nonsense transcripts 1 (UPF1). UPF1 is an ATP-dependent helicase that unwinds the double-stranded structure to facilitate the formation of polysome. Using sucrose density centrifugation, we found that knockdown of STAU1 inhibited polysome formation in FABP4 mRNA. Distribution of FABP4 mRNA was also altered by the knockdown of

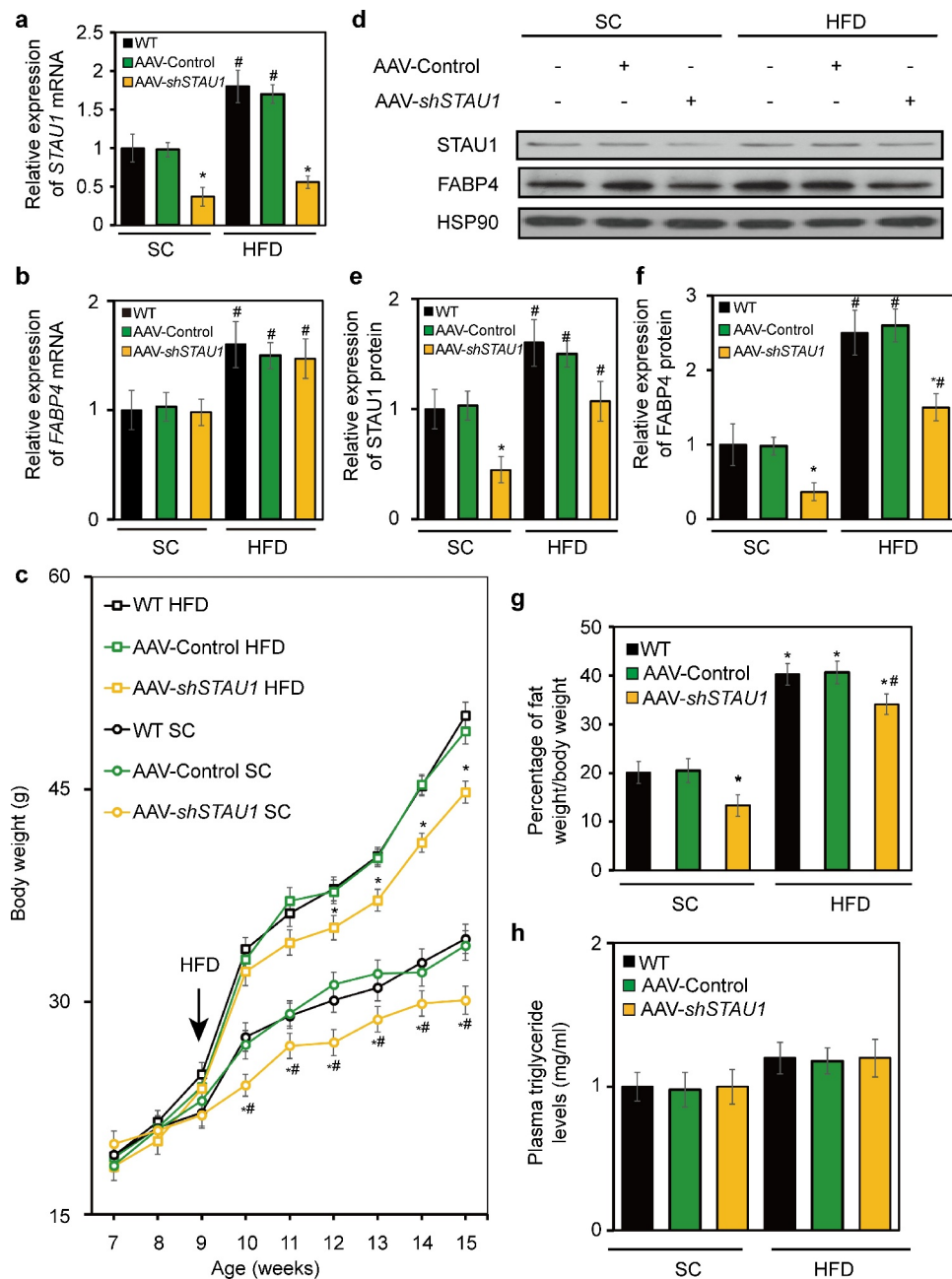


**Figure 5.** Effect of STAU1 knockdown on body weight and lipid metabolism in diet-induced obese mice. Gene expression analysis was performed using adipose tissue from mice fed standard chow (SC) and high-fat diet (HFD). The real-time PCR analysis of *STAU1* (a) and *FABP4* (b) mRNA expression relative to that of wild type SC-fed mice (3–5 animals per group). C: Bodyweight per mouse of groups fed HFD or SC diet and treated with AAV-control or AAV-shSTAU1. D: Western blot showing STAU1 and FABP4 expression in wild type SC- and HFD-fed mice after downregulation of STAU1. E–F: Quantification of STAU1 and FABP4 (f) protein levels relative to that of wild-type SC-fed mice. G: Nuclear magnetic resonance (NMR) analysis of body fat composition presented as percentage of body weight. \*Represents a significant difference between wild-type group and AAV-control group or AAVshSTAU1 group of SC-fed mice. #Represents a significant difference between wild-type group and AAV-control group or AAVshSTAU1 group of HFD-fed mice.

*STAU1*. We treated 3T3-L1 cells with OA to retain UPF1 in a hyperphosphorylated state. Our results indicate that maintaining UPF1 in a hyperphosphorylated state increases FABP4 expression at the protein level but not at the mRNA level. While expression of FABP4 was decreased by the downregulation of STAU1, the

expression levels of PPAR $\gamma$  were increased. These results agree with those obtained by Tali et al., showing that FABP4 attenuated the expression of PPAR $\gamma$  and promoted its degradation [17].

FABP4 has a higher affinity and selectivity for long-chain fatty acids and facilitates the transportation of

fatty acids to several cellular organelles [27]. Our analysis of the FFA content in the cell media indicated that the downregulation of STAU1 dramatically decreased the transportation of fatty acids; this result agreed with those obtained via oil red O staining. Downregulation of STAU1 also decreased the formation of lipid droplets within cells. These data show that STAU1 regulated adipogenesis *in vitro*. To downregulate the expression of STAU1 *in vivo* using AAV-encoded shRNA, we injected AAV into the subcutaneous fat tissues of mice. Our results indicate that downregulation of STAU1 in the fat tissues decreased the body weights and adipose tissue ratio in our mouse cohorts. However, the AAV-induced downregulation of STAU1 did not change FFA levels in mouse plasma. This may have occurred because the effects of a local injection are often not robust enough to induce systemic effects in mice.

STAU1 is a ubiquitously expressed dsRNA binding protein that can detect the secondary structure of mRNA [22,28]. The most important function of STAU1 occurs in Staufen-mediated mRNA decay (SMD). In the SMD pathway, STAU1 detects the double-stranded structure in the 3' UTR of mRNA and recruits other RNA-binding proteins (RBPs) to degrade the mRNA [29]. STAU1 can also recognize the double-stranded structure in CDS and facilitate translation [30]. One study has shown that STAU1 can regulate the expression of MyoD at the translational level in quiescent MuSCs [7]. In this study, we have shown that STAU1 can regulate the translation of FABP4 during adipogenesis. Nonsense-mediated mRNA decay and SMD are competitive pathways [11]. STAU1 competes with UPF2 for binding to UPF1 and promotes the SMD pathway. Our results indicate that STAU1 may regulate alternative splicing (AS) events during adipogenesis (data not shown). In conclusion, we have shown that STAU1 regulates adipogenesis via binding to key mRNAs during adipogenesis and modifying these mRNAs by regulating AS, translation, or SMD.

RBPs play various roles in adipogenesis and obesity [31,32]. Among these RBPs, double-stranded RBPs are challenging to study because the binding of dsRNA-binding proteins is dependent on the secondary structure of RNA [33]. STAU1 is a typical dsRNA-binding protein; the RNAs bound by STAU1 differ in their fates and destinations. As described previously in this study, the many functions of STAU1 are mainly influenced by the position of SBS. Future studies may clarify which transcripts are bound by STAU1 during adipogenesis.

## Methods

### Chemicals, siRNAs, cell culture, and transfection

The mouse 3T3-L1 cells used in this study were acquired from the American Type Culture Collection (ATCC, Manassas, VA, USA). The 3T3-L1 cells were cultured to confluence in Dulbecco's Modified Eagle's Medium (DMEM; Gibco) supplemented with 10% foetal calf serum (FBS; Gibco, Grand Island, NY, USA). Okadaic acid (OA; Sigma-Aldrich) was dissolved in dimethyl sulphoxide (DMSO; Sangon) and used to treat the cells at a final concentration of 0.1  $\mu$ M 4 days post-transduction. 3T3-L1 cells were then transiently transfected with siRNAs using Lipofectamine 3000 (Invitrogen) according to manufacturer's instructions, at indicated time points, and harvested 2 days post-transfection. Total RNA was purified using TRIzol (Invitrogen), and total protein was extracted with cell lysis buffer (Thermo Fisher Scientific) containing a cOmplete™ ULTRA Tablets, Mini, EASYpack protease inhibitor (Roche).

Two siRNAs targeting STAU1 were synthesized by Sangon Biotech according to a previous study, siRNA1: 5'-r (CAACUGUACUACCUUUCCA) d (TT)-3'; siRNA2: 5'-r (AACGGU AACUGCCAUGAUA) d (TT)-3' [18].

### Animals

All animal care and experimental procedures in this study were approved by the Animal Experimentation Ethics Committee of Xinjiang Medical University (approval number: 20,170,214–156). Animal study protocols complied with the ARRIVE guidelines and were carried out in accordance with the National Institutes of Health guide for the care and use of laboratory animals (NIH Publications No. 8023, revised 1978). Male C57Bl/6 J mice (4–5 weeks old) used in this study were obtained from the Experimental Animal Center of Xinjiang Medical University. Mice were housed in groups of 3–4 under standard housing conditions on a 12 h light/dark cycle and provided with *ad libitum* access to water and a standard chow diet until 9 weeks of age. Half of the mice were then switched to a high-fat diet (HFD), which was administered for an additional 11 weeks. Bodyweight and food intake were monitored weekly. Body fat composition was analysed using a Fat/Lean MiniQMR (Niumag, Suzhou, Jiangsu, China) at week 11 of the HFD.



## Adipogenesis, oil red O staining, and quantification of stained oil droplets

Murine 3T3-L1 cells were cultured in DMEM containing 10% FBS; the cell suspension was adjusted to approximately  $1 \times 10^5$  cells/mL. After 48 h, the cells were treated with an induction cocktail containing 10  $\mu$ g/mL insulin (Sigma-Aldrich), 115  $\mu$ g/mL 3-isobutyl-1-methylxanthine (Sigma-Aldrich), and 3.9  $\mu$ g/mL dexamethasone (Thermo Fisher Scientific). The cells were then allowed to incubate until differentiation was observed, and the degree of differentiation was assessed at different time points.

To detect the accumulated lipid droplets, differentiated 3T3-L1 cells were washed three times with PBS and fixed using 4% paraformaldehyde (Thermo Fisher Scientific) for 2 h at 22–27°C. The cells were then stained with 60% oil red O (Thermo Fisher Scientific) for 30 min and washed with PBS. To quantitate the stained triglycerides, the cells were dissolved in isopropanol for 10 min and then evaluated at 495 nm with an Agilent Cary 3500 spectrophotometer (Agilent Technologies, Santa Clara, CA, USA).

### Quantitative real-time PCR

Total RNA was harvested from cells or tissues at different time points. Quality and the concentration of RNA were measured using a Nanodrop Spectrophotometer (Thermo Fisher Scientific, Waltham, MA, USA). cDNA was prepared using a SuperScript III Reverse Transcription Kit (Thermo Fisher Scientific) according to the manufacturer's instructions. qRT-PCR was performed on an ABI 7500 (Applied Biosystems, Waltham, MA, USA) using SYBR-Green PCR kit I (Applied Biosystems) according to the manufacturer's instructions. The primers used for *STAU1*, *FABP4*, *PPAR $\gamma$* , *CEBP $\alpha$* , *HSP90*, and *GAPDH* mRNA have been previously described [34].

### Western blotting

A total of 50  $\mu$ g of each of the samples was loaded into each lane of 12% SDS-PAGE gels, transferred to nitrocellulose membranes (Bio-Rad, Hercules, CA, USA), blocked with 5% bovine serum albumin, and probed with primary antibodies overnight. Antibodies were used at concentrations recommended by their respective manufacturers. For this procedure, we used primary antibodies against HSP90 (Cat: BM4191, Boster, Wuhan, Hubei, China), mouse STAU1 (Cat: ab73478, Abcam, Cambridge, MA, USA), mouse FABP4 (Abcam, Cambridge, MA, USA), mouse PPAR $\gamma$  (Cat: ab66682,

Abcam, Cambridge, MA, USA), and mouse CEBP $\alpha$  (Cat: sc-365,318, Santa Cruz, Santa Cruz, CA, USA). The membranes were first incubated with the primary antibodies overnight at 22–27°C and then with horseradish peroxidase-conjugated secondary antibodies (Cat: BA1077, Goat Anti-Mouse IgG (H + L) Secondary Antibody, HRP Conjugate; Cat: BA1054, Goat Anti-Rabbit IgG (H + L) Secondary Antibody, HRP Conjugate, Boster, Wuhan, Hubei, China). The signal was detected via chemiluminescence using an ECL kit (Bio-Rad). Densitometric analysis was performed using Image Lab software (Bio-Rad, Hercules, CA, USA).

### Sucrose density centrifugation

3T3-L1 cells were lysed using RIPA buffer. The extracts were cleared through centrifugation for 10 min at  $12,000 \times g$  and loaded onto a continuous 15%–40% sucrose gradient. Fifteen fractions were collected after centrifugation for 16 h at  $83,000 \times g$ . To assess poly-some proliferation, the absorption of each fraction was determined at 254 nm by an Agilent Cary 3500 spectrometer. To determine the distribution of *FABP4* mRNA, total RNA was extracted from each fraction using a phenol: chloroform: isopropanol mixture.

### RNA immuno-precipitation and photoactivatable ribonucleotide enhanced crosslinking and immunoprecipitation

RNA immune-precipitation (RIP) was conducted using an RNA Immunoprecipitation Kit (Millipore, Billerica) per manufacturer's instructions. Lysed 3T3-L1 cells were incubated overnight with 10  $\mu$ L of STAU1 antibody and then precipitated using 30  $\mu$ L A/G agarose beads (GE, Little Chalfont, Buckinghamshire, UK). After precipitation, RNA was extracted using the phenol: chloroform: isoprene mixture.

3T3-L1 cells at 80% confluence were then evaluated using a PAR-CLIP assay. For this, the cells were treated with 100  $\mu$ M 4-thiouridine (SU, Sigma-Aldrich), incubated at 37°C for 16 h, and then irradiated with 150 mJ/cm<sup>2</sup>, 365 nm ultraviolet light in a UV crosslinker (CL-1000 L, UVP, USA) to facilitate crosslinking of RNA with STAU1. Cellular lysates were prepared and incubated with RNase T1 at the final concentration of 1 U/ $\mu$ L in a water bath for 15 min at 22°C. Protein G magnetic beads were incubated with anti-STAU1 antibody (Cat: ab73478, Abcam, Cambridge, MA, USA) or IgG. Next, the mRNA-STAU1 complex was isolated from the lysate by immunoprecipitation. A second RNase T1

digestion ensured that only the RNA segment that was bound and protected by STAU1 was detected. RNA was extracted using a phenol: chloroform: iso-pentane mixture. Primers for each section of the *FABP4* mRNA were designed, and exact binding sites of STAU1 protein and *FABP4* mRNA were detected via qPCR.

### Administration of recombinant AAV vectors

Single-stranded AAV vectors were produced via triple transfection of human embryonic kidney 293 cells and purified using a CsCl-based gradient described previously [35]. The AAV-*shSTAU1* was targeted to mouse *STAU1* mRNA carrying the same sequence as siRNA1 used *in vitro* as described previously in the ‘Chemicals, siRNAs, cell culture, and transfection’ section of the Methods.

Mice were anesthetized with ketamine (100 mg/kg) and xylazine (10 mg/kg). A laparotomy was performed for the intraepididymal (intrae) delivery of white adipose tissue (WAT). To distribute the vector in the whole depot, each epididymal fat pad was injected twice with 500  $\mu$ L of AAV-containing solution.

### Plasma analysis

Plasma TG and free fatty acid levels were measured using a commercial kit (Cat: KT37563, MSK) and half micro-test (Cat: KT21006, MSK), respectively, according to the manufacturer’s instructions.

### Statistical analysis

The Student’s *t*-test (two-tailed) and one-way ANOVA were conducted to analyse the *in vivo* and *in vitro* data using SPSS 19.0 (IBM, New York, USA). Data are expressed as the mean  $\pm$  standard deviation. The hypotheses were tested by calculating the 95% confidence interval or by one-way or two-way ANOVA statistical tests.  $P < 0.05$  was considered statistically significant.

### Disclosure statement

No potential conflict of interest was reported by the authors.

### Funding

This work was supported by Xinjiang Uygur Autonomous Region Natural Science Fund [grant number: 2017D01C179]. The funding agency had no influence on the design, implementation, or interpretation of this study. The funding

agency did not participate in the writing of this manuscript or submission of this manuscript for publication.

### Author contributions

YG and XL conceived the research concept and designed the experiments. XL, YJ, YX, and TH carried out the experiments. XL and XG collected and analysed the data. XL and XM interpreted the data. All authors were involved in writing the paper. XL, YJ, and YG approved the final version of the paper.

### ORCID

Xiaodi Liang  <http://orcid.org/0000-0002-5484-5127>  
Yaquun Guan  <http://orcid.org/0000-0002-5729-9889>

### References

- Ghaben AL, Scherer PE. Adipogenesis and metabolic health. *Nat Rev Mol Cell Biol.* 2019;20:242–258.
- Lee JE, Schmidt H, Lai B, et al. Transcriptional and epigenomic regulation of adipogenesis. *Mol Cell Biol.* 2019;39:e00601–e00618.
- Mota de Sa P, AJ R, Hang H, et al. Transcriptional regulation of adipogenesis. *Compr Physiol.* 2017;7:635–674.
- Rosen ED, Walkey CJ, Puigserver P, et al. Transcriptional regulation of adipogenesis. *Genes Dev.* 2000;14:1293–1307.
- Denny SK, Bisaria N, Yesselman JD, et al. High-throughput investigation of diverse junction elements in RNA tertiary folding. *Cell.* 2018;174:377–390 e320.
- Ramanouskaya TV, Grinev VV. The determinants of alternative RNA splicing in human cells. *Mol Genet Genomics.* 2017;292:1175–1195.
- de Morree A, Ctj VV, Gan Q, et al. Stau1 inhibits MyoD translation to actively maintain muscle stem cell quiescence. *Proc Natl Acad Sci U S A.* 2017;114:E8996–E9005.
- Kim MY, Park J, Lee JJ, et al. Stau1-mediated mRNA decay induces Requiem mRNA decay through binding of Stau1 to the Requiem 3’UTR. *Nucleic Acids Res.* 2014;42:6999–7011.
- Martel C, Dugre-Brisson S, Boulay K, et al. Multimerization of Stau1 in live cells. *RNA.* 2010;16:585–597.
- Ricci EP, Kucukural A, Cenik C, et al. Stau1 senses overall transcript secondary structure to regulate translation. *Nat Struct Mol Biol.* 2014;21(1):26–35.
- Cho H, Kim KM, Han S, et al. Stau1-mediated mRNA decay functions in adipogenesis. *Mol Cell.* 2012;46:495–506.
- Villeneuve J, Bassaganyas L, Lepreux S, et al. Unconventional secretion of FABP4 by endosomes and secretory lysosomes. *J Cell Biol.* 2018;217:649–665.
- Furuhashi M. Fatty acid-binding protein 4 in cardiovascular and metabolic diseases. *J Atheroscler Thromb.* 2019;26:216–232.
- Distel RJ, Robinson GS, Spiegelman BM. Fatty acid regulation of gene expression. *Transcriptional and*

- post-transcriptional mechanisms. *J Biol Chem.* **1992**;267:5937–5941.
- [15] Scifres CM, Chen B, Nelson DM, et al. Fatty acid binding protein 4 regulates intracellular lipid accumulation in human trophoblasts. *J Clin Endocrinol Metab.* **2011**;96:E1083–1091.
- [16] Ayers SD, Nedrow KL, Gillilan RE, et al. Continuous nucleocytoplasmic shuttling underlies transcriptional activation of PPARgamma by FABP4. *Biochemistry.* **2007**;46:6744–6752.
- [17] Garin-Shkolnik T, Rudich A, Hotamisligil GS, et al. FABP4 attenuates PPARgamma and adipogenesis and is inversely correlated with PPARgamma in adipose tissues. *Diabetes.* **2014**;63:900–911.
- [18] Kim YK, Furic L, Desgroseillers L, et al. Mammalian Stau1 recruits Upf1 to specific mRNA 3'UTRs so as to elicit mRNA decay. *Cell.* **2005**;120:195–208.
- [19] Gruber AR, Lorenz R, Bernhart SH, et al. The Vienna RNA websuite. *Nucleic Acids Res.* **2008**;36:W70–74.
- [20] Isken O, Kim YK, Hosoda N, et al. Upf1 phosphorylation triggers translational repression during nonsense-mediated mRNA decay. *Cell.* **2008**;133:314–327.
- [21] Chen YM, Ou BT, Chen CY, et al. Stau1 protein participates positively in the viral RNA replication of enterovirus 71. *Viruses.* **2019**;11:E142.
- [22] Paul S, Dansithong W, Figueroa KP, et al. Stau1 links RNA stress granules and autophagy in a model of neurodegeneration. *Nat Commun.* **2018**;9:3648.
- [23] Rouskin S, Zubradt M, Washietl S, et al. Genome-wide probing of RNA structure reveals active unfolding of mRNA structures in vivo. *Nature.* **2013**;505:701–705.
- [24] Floresta G, Pistara V, Amata E, et al. Adipocyte fatty acid binding protein 4 (FABP4) inhibitors. A comprehensive systematic review. *Eur J Med Chem.* **2017**;138:854–873.
- [25] Kramer MC, Gregory BD. Does RNA secondary structure drive translation or vice versa? *Nat Struct Mol Biol.* **2018**;25:641–643.
- [26] Pan X, Rijnbeek P, Yan J, et al. Prediction of RNA-protein sequence and structure binding preferences using deep convolutional and recurrent neural networks. *BMC Genomics.* **2018**;19:511.
- [27] Furuhashi M, Fuseya T, Murata M, et al. Local production of fatty acid-binding protein 4 in epicardial/perivascular fat and macrophages is linked to coronary atherosclerosis. *Arterioscler Thromb Vasc Biol.* **2016**;36:825–834.
- [28] Lazzaretti D, Bandholz-Cajamarca L, Emmerich C, et al. The crystal structure of Stau1 in complex with a physiological RNA sheds light on substrate selectivity. *Life Sci Alliance.* **2018**;1:e201800187.
- [29] Lebeau G, Maher-Laporte M, Topolnik L, et al. Stau1 regulation of protein synthesis-dependent long-term potentiation and synaptic function in hippocampal pyramidal cells. *Mol Cell Biol.* **2008**;28:2896–2907.
- [30] Kim YK, Furic L, Parisien M, et al. Stau1 regulates diverse classes of mammalian transcripts. *EMBO J.* **2007**;26:2670–2681.
- [31] Xu D, Xu S, Kyaw AMM, et al. RNA binding protein Ybx2 regulates RNA stability during cold-induced brown fat activation. *Diabetes.* **2017**;66:2987–3000.
- [32] Hentze MW, Castello A, Schwarzl T, et al. A brave new world of RNA-binding proteins. *Nat Rev Mol Cell Biol.* **2018**;19:327–341.
- [33] Lim GH, Hoey T, Zhu S, et al. COP1, a negative regulator of photomorphogenesis, positively regulates plant disease resistance via double-stranded RNA binding proteins. *PLoS Pathog.* **2018**;14:e1006894.
- [34] Jiao Y, Liang X, Hou J, et al. Adenovirus type 36 regulates adipose stem cell differentiation and glucolipid metabolism through the PI3K/Akt/FoxO1/PPARgamma signaling pathway. *Lipids Health Dis.* **2019**;18:70.
- [35] Ayuso E, Mingozzi F, Montane J, et al. High AAV vector purity results in serotype- and tissue-independent enhancement of transduction efficiency. *Gene Ther.* **2010**;17:503–510.